ISSN 1063-7737, Astronomy Letters, 2018, Vol. 44, No. 3, pp. 149–161. © Pleiades Publishing, Inc., 2018.
Original Russian Text © A.E. Shtykovsky, V.A. Arefiev, A.A. Lutovinov, S.V. Molkov, 2018, published in Pis'ma v Astronomicheskii Zhurnal, 2018, Vol. 44, No. 3, pp. 173–186.

Peculiarities of Super-Eddington Flares from the X-ray Pulsar LMC X-4 Based on NuSTAR Data

A. E. Shtykovsky*, V. A. Arefiev, A. A. Lutovinov, and S. V. Molkov

Space Research Institute, Russian Academy of Sciences, Profsoyuznaya ul. 84/32, Moscow, 117997 Russia

Received June 27, 2017

Abstract—We present the results of our analysis of super-Eddington flares recorded from the X-ray pulsar LMC X-4 by the NuSTAR observatory in the energy range 3–79 keV. The pulsar spectrum is well described by the thermal Comptonization model (COMPTT) both in quiescence and during flares, when the peak luminosity reaches $L_x \sim (2–4) \times 10^{39}$ erg s^{-1}. An important feature that has been investigated for the first time in this paper is that an increase in luminosity during flares by more than an order of magnitude is observed at energies below 25–30 keV, while at higher energies (30–70 keV) the spectrum shape and the source flux remain virtually unchanged. The increase in luminosity is accompanied by changes in the source pulse profile—in the energy range 3–40 keV it becomes approximately triangular and the pulsed fraction increases with rising energy, reaching 60–70% in the energy range 25–40 keV. We discuss possible changes in the geometry of the accretion column consistent with similar changes in the spectra and pulse profiles.

DOI: 10.1134/S1063773718030015

Keywords: *X-ray pulsars, neutron stars, accretion, LMC X-4.*

INTRODUCTION

LMC X-4 is a high-mass X-ray binary system located in the Large Magellanic Cloud (its distance is $d = 50$ kpc) with a spin period $P_{spin} \sim 13.5$ s and an orbital period $P_{orb} \simeq 1.4$ days. The system consists of a neutron star with a mass $M_\star \simeq 1.57\ M_\odot$, where $M_\odot$ is the solar mass, and an optical companion, an O8 III star with a mass of $\sim 18\ M_\odot$ (see, e.g., Falanga et al. 2015, and references therein). X-ray observations show the presence of X-ray eclipses in the LMC X-4 system (Li et al. 1978; White 1978) and an X-ray flux modulation with a period $P_{sup} \simeq 30.5$ days (superorbital period) associated with the periodic obscuration of the X-ray source by a precessing accretion disk (Lang et al. 1981; Heemskerk and van Paradijs 1989; Neilsen et al. 2009). The observed X-ray intensity of the source changes on the scale of the superorbital cycle by a factor of $\sim$50 (for more details, see Heemskerk and van Paradijs 1989). The intrinsic X-ray luminosity of the pulsar remains approximately constant (given the local fluctuations) with $L_x \sim (2–5) \times 10^{38}$ erg s^{-1} (Levine et al. 2001; Tsygankov and Lutovinov 2005; Molkov et al. 2015; Shtykovsky et al. 2017, and references therein), which corresponds to or slightly exceeds the Eddington limit for a neutron star with a mass of $\sim 1.57\ M_\odot$.

Transient increases in X-ray luminosity called X-ray bursts or flares are commonly observed in close binary systems with compact objects. Such flares can be different in nature—in particular, they can arise from thermonuclear explosions, nonstationary accretion, etc. In LMC X-4 flaring activity has been recorded in X-rays virtually since its discovery (Kelley et al. 1983; Dennerl 1989; Levine et al. 1991, 2000; Moon et al. 2003), with flares being recorded in both high and low states (Woo et al. 1996). Flares are observed as episodic super-Eddington luminosity events ($\sim 10^{39}–10^{40}$ erg s^{-1}) lasting up to several thousand seconds (Levine et al. 2000; Moon et al. 2003). The pulsar flaring activity does not have a regular pattern and is apparently aperiodic in character (Levine et al. 2000). The light curves during flares are modulated with the spin period (Kelley et al. 1983; Levine et al. 2000; Moon and Eikenberry 2001). Thus far, no exhaustive physical theory (mechanism) explaining the nature, energetics, and timing properties of flares from LMC X-4 has been proposed. Studying the flaring activity is of great interest from the viewpoint of the physical processes occurring in the source, because it involves the accumulation of large stores of energy, the development of nonstationary processes leading to the release of this energy in a short time, and the accompanying dynamical activity of the pulsar. A high luminosity

*E-mail: a.shtykovsky@iki.rssi.ru

Table 1. NuSTAR observations of LMC X-4

ObsID	Ψ_{orb}	Ψ_{sup}	Start time (MJD)	Exposure, s
30102041002	[0.29; 0.63]	[0.88; 0.89]	Oct. 30, 2015, 01:01:08 (57325.0425)	24 551
30102041004	[0.39; 0.69]	[0.07; 0.08]	Nov. 4, 2015, 19:46:08 (57330.8237)	21 880
30102041006	[0.11; 0.43]	[0.28; 0.30]	Nov. 11, 2015, 11:16:08 (57337.4695)	22 986
30102041008	[0.42; 0.73]	[0.81; 0.82]	Nov. 27, 2015, 09:16:08 (57353.3862)	20 282

of the source during flares (up to $\sim 10^{40}$ erg s^{-1}) is especially intriguing in this aspect, which may allow LMC X-4 to be called a flaring ultraluminous source.

In this paper we have performed a detailed analysis of the source emission at various orbital and superorbital phases in a wide energy range for the first time using NuSTAR data. Special attention in our analysis has been given to the X-ray flaring activity recorded during observations.

OBSERVATIONS AND DATA REDUCTION

In this paper we analyze the data obtained by the NuSTAR observatory (Harrison et al. 2013) during the observations of the pulsar LMC X-4 in October and November 2015 (ObsID 30102041002, 30102041004, 30102041006, and 30102041008). The observations cover various orbital (Ψ_{orb}) and superorbital (Ψ_{sup}) cycles of the system (Molkov et al. 2015). The exposure time in the science mode (mode 01) in each observation was $\sim$20–25 ks (Table 1).

The primary data reduction was carried out with the standard NuSTAR data analysis software (NUSTARDAS, version 1.5.1) using the CALDB calibration database (version 20160922). The high-level data reduction and analysis were performed with the HEASOFT software package (version 6.18). The photon arrival times were corrected for the Solar system barycenter using the standard NUSTARDAS tools. The corresponding correction of the photon arrival times for the motion of the compact object in the binary system was made using the orbital parameters from Molkov et al. (2015).

To construct the light curves, the background was subtracted from the data of each of the FPMA and FPMB modules; the light curves obtained were combined into a single curve to which a correction for the orbital motion was applied (Krivonos et al. 2015). The standard LCMATH tool from the HEASOFT software package was used to combine the light curves of the NuSTAR modules.

We searched for the pulsation period using the epoch-folding technique (the EFSEARCH tool in the HEASOFT package; for more details on the applied technique, see the corresponding section). The pulse profiles in different energy ranges were constructed by folding the source's light curve with the period found. The energy spectra were analyzed using the XSPEC package (version 12.8).

RESULTS

Light Curves

The pulsar light curves in the energy range 3–79 keV for observations 30102041002 and 30102041008 are presented in Figs. 1 and 2, respectively. There are two episodes of flaring activity in these observations: one contains three events (FL1, FL2, and FL3); the other contains one event (FL4). The FL1, FL2, and FL3 events are spaced $\sim$10 ks apart. The episodes of flaring activity in observations 30102041002 and 30102041008 (the FL1 and FL4 events) are separated by a time interval of $\sim$28.3 days. The duration of each event is $\sim$4000 s. All flares (see, e.g., the lower panel in Fig. 1 for FL3 and the lower panel in Fig. 2 for FL4) shows a similar morphology: a fast rise, an exponential decay (characteristic time scales $t_{exp} \sim 800$–1200 s), an afterglow, pronounced pulsations at the pulsar spin frequency, and the presence of subpulses during the main flare and the afterglow. No flaring activity was observed in observations 30102041004 and 30102041006.

For the subsequent analysis the data from the observations containing flares were divided into intervals and marked by numbers. The intervals were chosen so as to separate the states with a high luminosity from the states with a normal one (this division is shown in Figs. 1 and. 2). The flares, in turn, were divided into two parts: the main flare and the afterglow (see, e.g., the lower panels in Figs. 1 and 2). The data from observations 30102041004 and 30102041006 were analyzed as a whole.

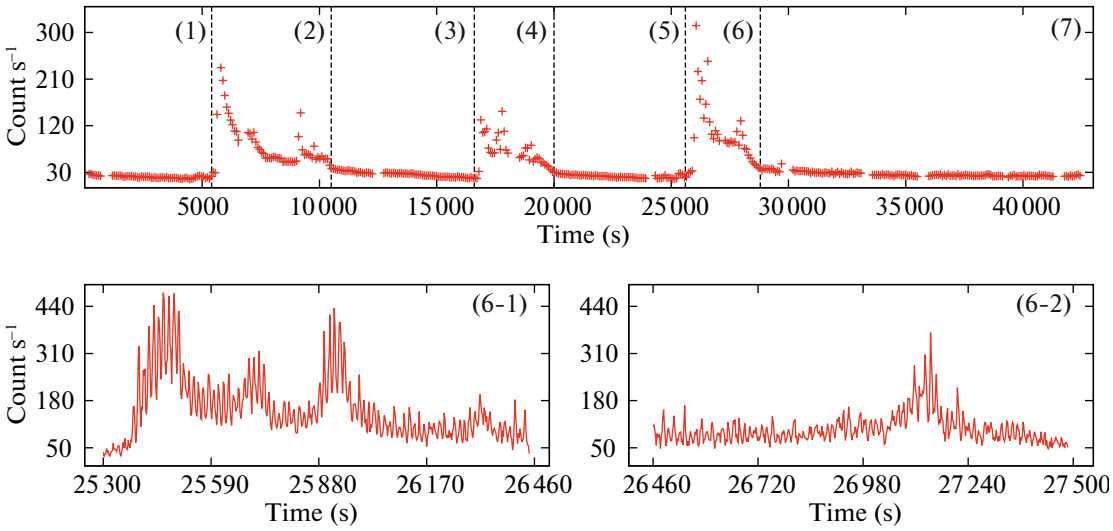

Fig. 1. (Color online) Light curve for observation 30102041002 (upper panel); light curve for the FL3 event in observation 30102041002, interval (6): the main flare (lower left panel, (6-1)) and the afterglow (lower right panel, (6-2)); for a detailed description, see the text. Zero time corresponds to the beginning of the observation (see Table 1).

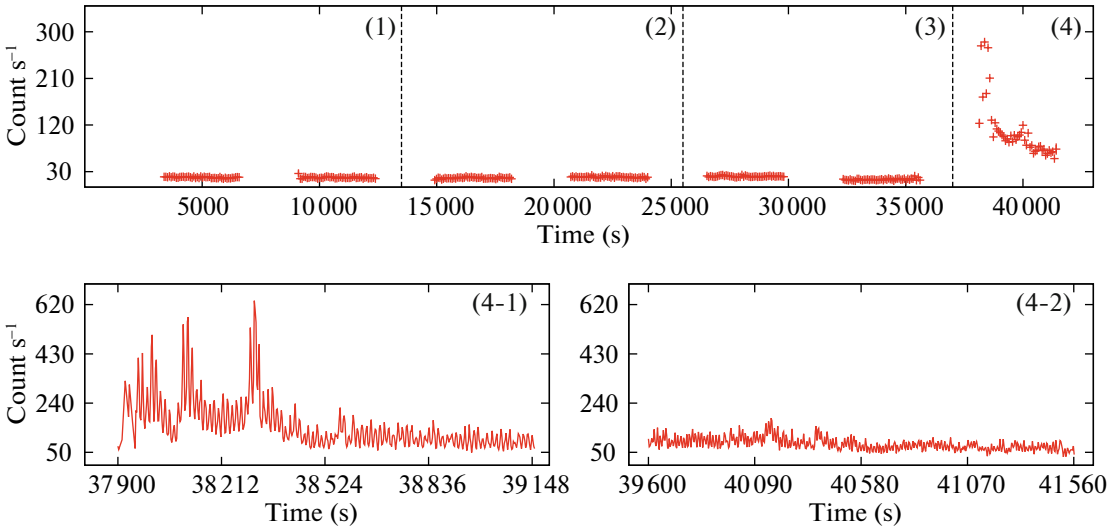

Fig. 2. (Color online) Light curve for observation 30102041008 (upper panel); light curve for the FL4 event in observation 30102041008, interval (4): the main flare (lower left panel, (4-1)) and the afterglow (lower right panel, (4-2)); for a detailed description, see the text.

Spin Period and Pulse Profile

To determine the spin period of LMC X-4, we used its light curves in the quiescent state (observations 30102041004 and 30102041006) combined from both NuSTAR modules. We determined the true spin period by the multiple ($N = 10\,000$) generation of samples by the Monte Carlo method based on the available sample (for more details on the applied method, see Boldin et al. 2013). As a result, we obtained the spin period of the neutron star at the time of NuSTAR observations $P_{\rm spin} = 13.50124 \pm 0.00005$ s, which was used in the subsequent analysis. The measured spin period agrees well with the results of previous NuSTAR (Shtykovsky et al. 2017) and XRT/Swift (Molkov et al. 2017) measurements. This may suggest the absence of a significant spin-up/spin-down of the neutron star in LMC X-4 compared to the previous history of observations (Molkov et al. 2017).

The pulse profile carries important information

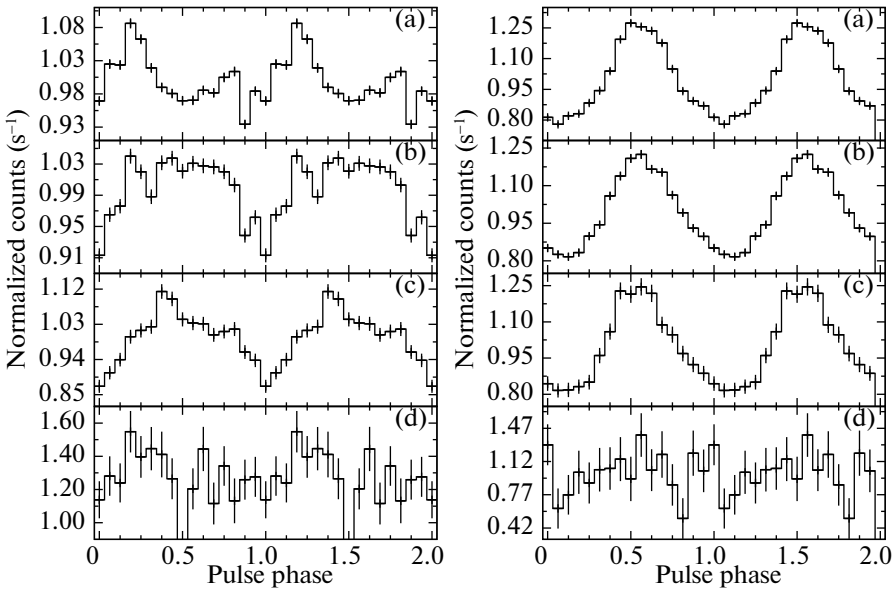

Fig. 3. Pulse profiles for observations 30102041004 (left panel) and 30102041006 (right panel) in the energy ranges 3–10 (a), 10–20 (b), 20–40 (c), and 40–79 keV (d).

about the geometry and physical properties of the pulsar emitting regions. A comparison of the profile shapes and their evolution in flares and quiescent states allows the processes during the pulsar flaring activity to be analyzed. Figures 3 (observations 30102041002 and 30102041006), 4 and 5 (observation 30102041002), and 6 (observation 30102041008) present the pulse profiles in the energy ranges 3–10, 10–20, 20–40, and 40–79 keV for each interval of observations described above. The same zero epoch $T_0 = 57325$ MJD was used to construct all pulse profiles.

In the absence of flaring activity, near the maximum of the superorbital period (observation 30102041004), the pulse profile has a complex shape consistent with previous observations (see, e.g., Levine et al. 2000; Shtykovsky et al. 2017). As the minimum of the superorbital period (observation 30102041006) is approached, the profile is simplified and approaches a sinusoidal shape (this is especially clearly seen in the energy ranges 3–10 and 10–20 keV), with the pulsed fraction increasing by a factor of ~3 (see Fig. 7).

The pulse profile approaches a regular triangular shape during flares and acquires a simple asymmetric shape similar to the sinusoidal one without pronounced features between flares. After the period of flaring activity the pulse profile returns to a complex shape that was recorded before flares and that is similar to the one observed during the maximum of the superorbital period (see, e.g., interval 7 in observation 30102041002 and intervals 1, 2, 3 in observation 30102041008). By analyzing the evolution of the pulse profiles in various intervals, we can see a pronounced drift of the pulse phase (to within the changes in the profile itself).

The energy dependence of the pulsed fraction differs significantly for the intervals of observations with flaring activity and the quiescent intervals (cf. the profiles in interval (6-1) of observation 30102041002 (Fig. 7a) and in observation 30102041004 (Fig. 7c)).

It can be seen from Fig. 7 that the pulsed fraction increases during the flares and reaches ~60–70% at energies 25–40 keV, which is much higher than the observed values of 6–14% in quiescence (Tsygankov and Lutovinov 2005; Shtykovsky et al. 2017). During the afterglow and immediately before the flare the pulsed fraction also reaches high values, ~25–50 and ~20–30%, respectively. Note that such changes in the profile are observed for all of the flares being analyzed in this paper. It should also be noted that in observation 30102041006, when the system was in the low state of the superorbital cycle, in the absence of flares, the pulsed fraction is also significantly higher than that in the high state and reaches ~20–30%. Lutovinov and Tsygankov (2009) showed that the pulsed fraction for bright X-ray pulsars must decrease with increasing luminosity. However, as it approaches or exceeds the Eddington limit, its increase can be observed again, as seen in LMC X-4.

Energy Spectra

As in our previous paper (Shtykovsky et al. 2017), the thermal Comptonization model COMPTT

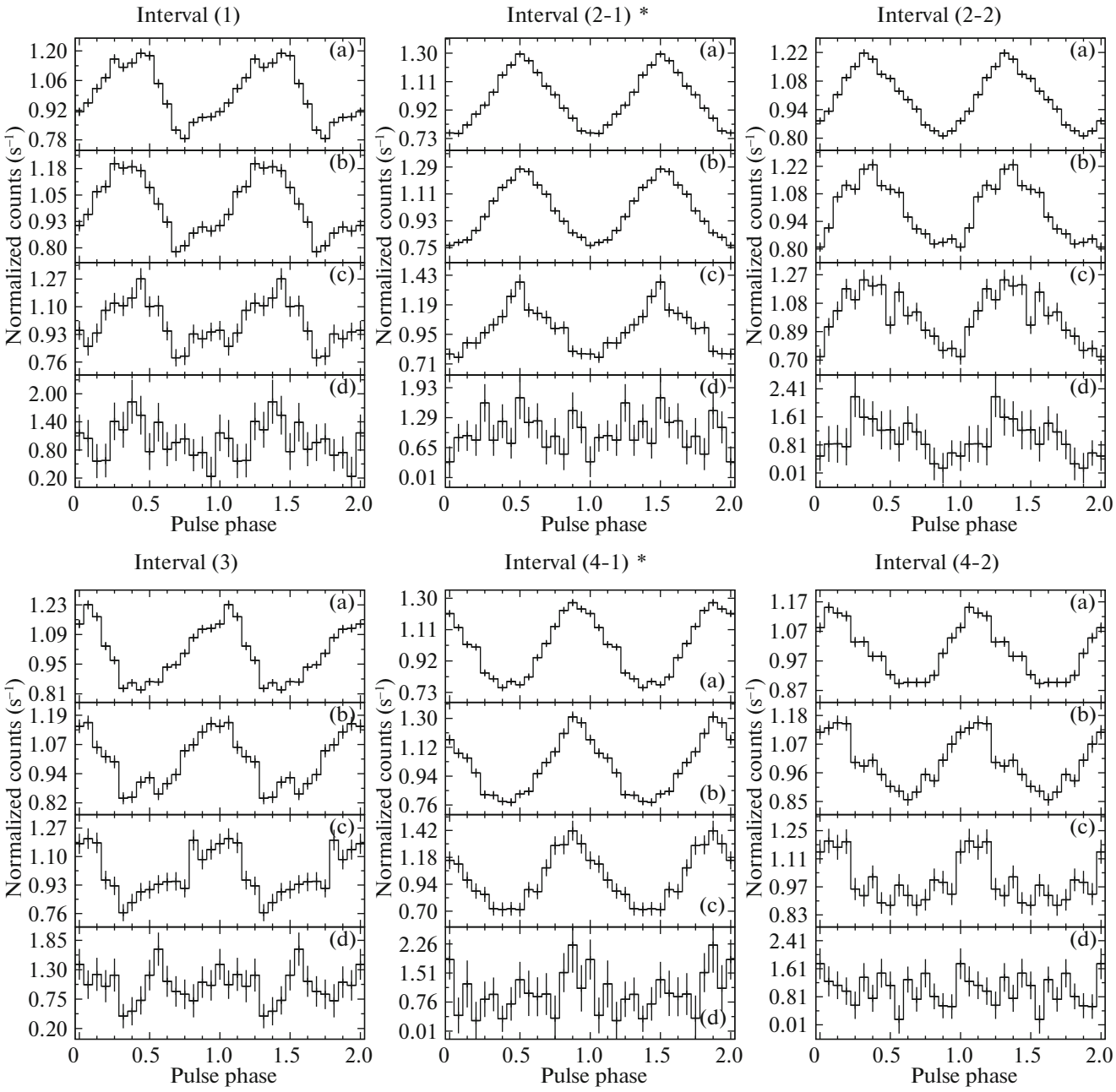

Fig. 4. Pulse profiles in intervals (1), (2-1), (2-2), (3), (4-1), and (4-2) (observation 30102041002) in the energy ranges 3–10 (a), 10–20 (b), 20–40 (c), and 40–79 keV (d); the intervals containing flares are marked by an asterisk (*).

(Titarchuk 1994) from the XSPEC package was used to fit the broadband spectra of LMC X-4. A significant advantage of this model is that it fits well the spectrum of LMC X-4 and has a physical justification. The following components were added to the model to improve the quality of the fit: PHABS to account for the interstellar absorption and GAUS to account for the fluorescent K_α iron line at 6.4 keV. The spectra from both modules were analyzed simultaneously, a normalization coefficient C was introduced to account for the difference between their calibrations, and all the remaining parameters were fixed between the data sets. The quality of the fit was estimated using the χ^2 test per degree of freedom (d.o.f.). The hydrogen column density was fixed at $N_{\rm H} = 5.74 \times 10^{20}$ atoms cm^{-2} (assuming a solar abundance Dickey and Lockman, 1990). The best-fit parameters are presented in Table 2. It can be seen

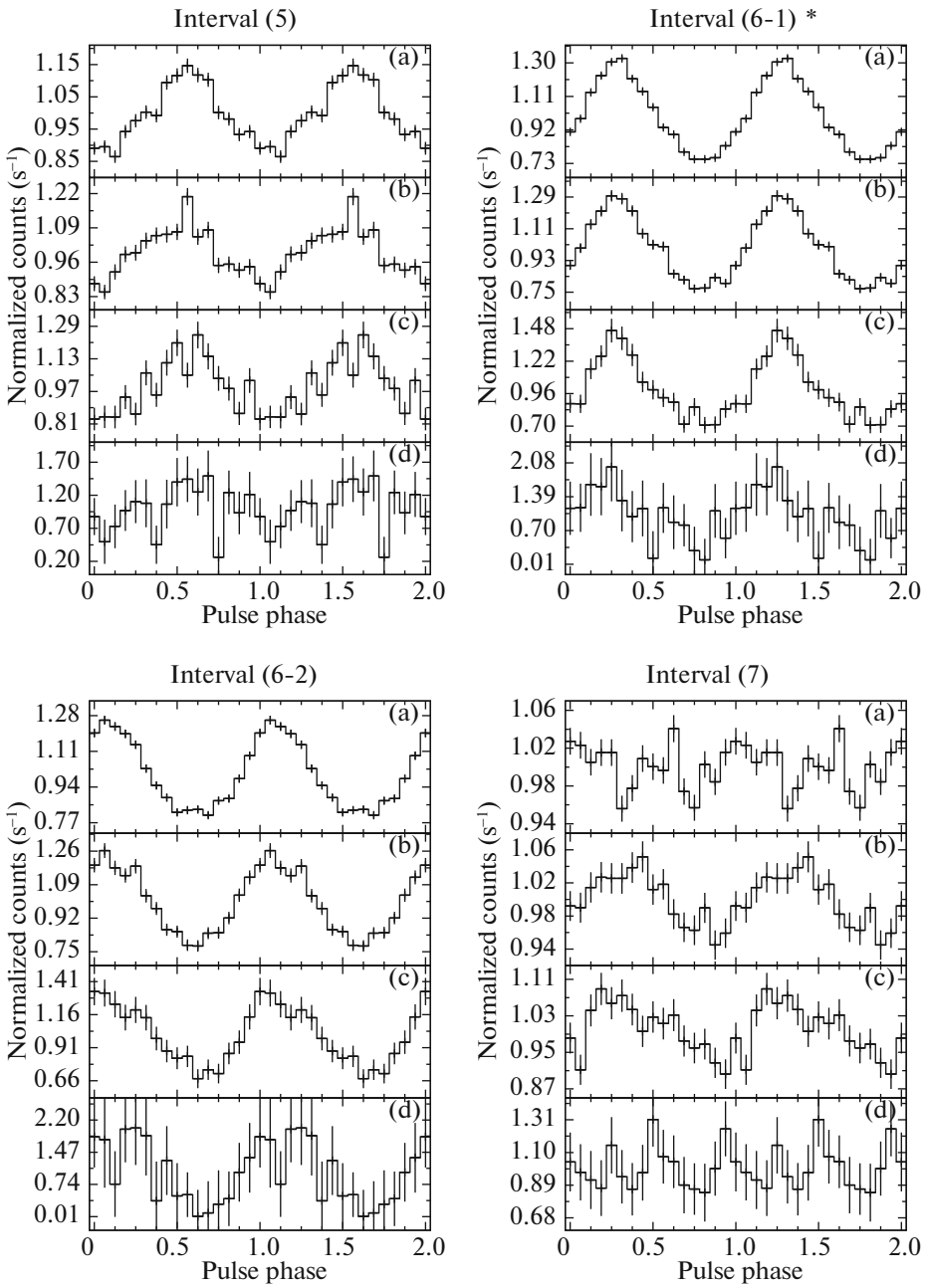

Fig. 5. Pulse profiles in intervals (5), (6-1), (6-2), and (7) (observation 30102041002) in the energy ranges 3–10 (a), 10–20 (b), 20–40 (c), and 40–79 keV (d); the intervals containing flares are marked by an asterisk (*).

from this table that the proposed model describes well the pulsar spectrum in all of the observed states.

Figure 8 presents the energy spectra of LMC X-4 before, during, and after the flare constructed simultaneously for each of the four flares. For clarity, the spectra before and after the flare were multiplied by coefficients of 0.1 and 0.2, respectively. It follows from the figure that during the flares the spectrum softens significantly. The spectral softening during flares in LMC X-4 was noted previously in a number of papers (see, e.g., Dennerl 1989; Levine et al. 1991, 2000; Moon et al. 2003). It can be seen from our data that the spectrum changes most dramatically at low energies. To test this assumption, we simultaneously constructed the spectra in the intervals containing flares and in the intervals preceding them (see Fig. 9). It can be seen from the figure that during the flares the shape of the spectrum changes predominantly up to ~20 keV, while at higher energies it remains virtually unchanged.

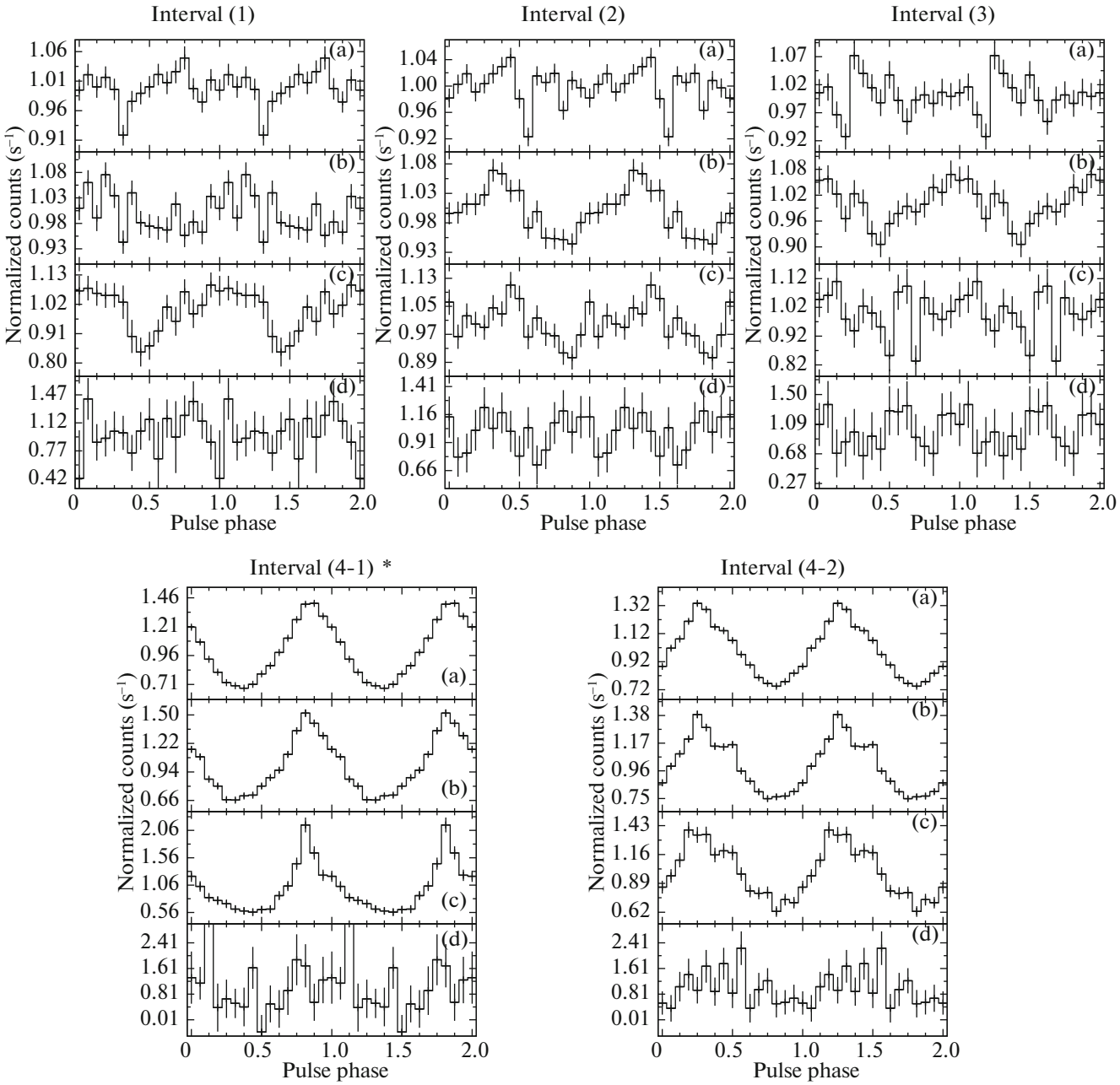

Fig. 6. Pulse profiles in intervals (1), (2), (3), (4-1), and (4-2) (observation 30102041008) in the energy ranges 3–10 (a), 10–20 (b), 20–40 (c), and 40–79 keV (d); the intervals containing flares are marked by an asterisk (*).

Figure 10 presents the evolution of the spectral parameters in intervals (1–7) of observation 30102041002 and intervals (1–4) of observation 30102041008. It can be seen from the plots that the optical depth of the emitting region decreases significantly (by a factor of ~1.5–2) during the flare, while the temperature of free electrons drops during the afterglow. It can also be seen from the data that a gradual rise in the seed photon temperature occurs during the series of flares, which ceases after it ends. Note that at least during the first flare in the series (FL3, FL4) the equivalent width of the fluorescent iron line EW_{Fe} increases sharply.

DISCUSSION AND CONCLUSIONS

The episodes of flaring activity in LMC X-4 have been known for quite a long time. Flares are transient increases in pulsar luminosity occurring approximately once a day (see, e.g., Levine et al. 2000;

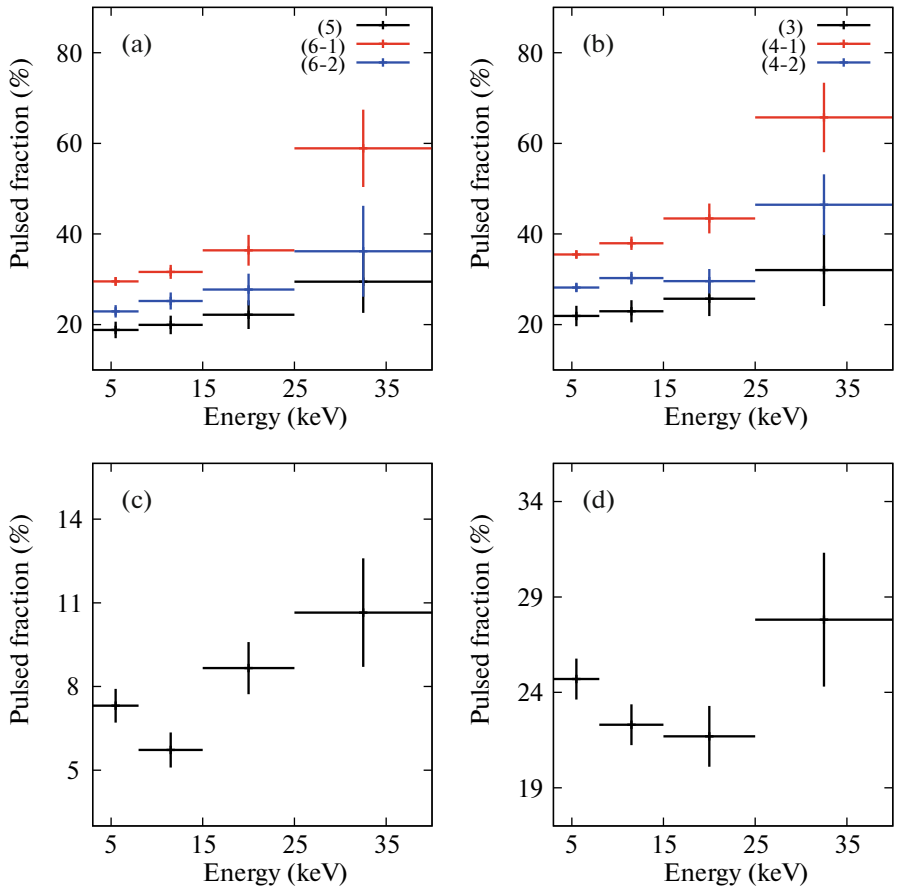

Fig. 7. (Color online) Pulsed fraction in the observations: 30102041002 in intervals (5), (6-1), and (6-2) (a); 30102041008 in intervals (3), (4-1), and (4-2) (b); 30102041004 (c); and 30102041006 (d).

Moon et al. 2003), but the regularity and flaring mechanism are not yet clear. Several models of flares in LMC X-4 have been proposed to date, each of which, nevertheless, has its shortcomings.

Flaring Activity

As has been said in the Introduction, flares in systems with accreting neutron stars can be caused by different physical mechanisms, among which the following can be noted: thermonuclear burning on the neutron star surface (type I bursts); accretion flow variability (type II bursts); nonstationary accretion (similar to what is observed in the so-called supergiant fast X-ray transients, SFXTs); and pulsar magnetospheric activity (magnetospheric perturbations).

Brown and Bildsten (1998) showed that the observed flares in LMC X-4 are difficult to explain in terms of the model of thermonuclear burning on the neutron star surface. In addition, thermonuclear flashes are characterized by a spectral softening as the flare develops, while in the case of flares in LMC X-4 the inverse process is observed—a spectral hardening as the flare evolves.

Another commonly considered mechanism for the appearance of flares is accretion flow variability. Let us first consider the simplest scenario whereby the accretion flow variations supply an additional amount of matter whose energy is released during accretion and raises the luminosity. Assuming that the efficiency of energy release by the infalling matter is $\eta \sim 10\%$, let us estimate the amount of matter that should be supplied to obtain the observed luminosities in FL3 (the average luminosity is $L_x = 7.27 \times 10^{38}$ erg s^{-1}) and FL4 (the average luminosity is $L_x = 8.14 \times 10^{38}$ erg s^{-1}). For this purpose, we will divide each of the flares into 200 s intervals and calculate the source flux in each interval using the spectral model described in the corresponding section. We will obtain the final mass by integration over all time intervals. The mass derived in this way is $M \simeq 1.8 \times 10^{22}$ g for FL3 and $M \simeq 2.3 \times 10^{22}$ g for FL4. Given the accretion rate in quiescence $\dot{m} \simeq 3.9 \times 10^{18}$ g s^{-1}, it is possible within this framework

Table 2. Parameters of the best-fit models for the spectra of LMC X-4 in various states

Observations	Interval	C	T_0, keV	kT, keV	τ	$E_{\rm Fe}$, keV	$\sigma_{\rm Fe}$, keV	$EW_{\rm Fe}$, eV	$f_{\rm x} \times 10^{-9}$, erg cm^{-2} s^{-1}	$\chi^2/d.o.f$
*02	(1)	1.02	0.93 ± 0.09	8.78 ± 0.10	12.29 ± 0.17	6.45 ± 0.05	0.44 ± 0.09	254 ± 28	0.68	0.995
	(2-1)	1.03	1.08 ± 0.06	8.78 ± 0.40	6.32 ± 0.32	6.32 ± 0.14	1.19 ± 0.16	644 ± 146	2.47	1.001
	(2-2)	1.02	1.00 ± 0.06	7.60 ± 0.10	11.24 ± 0.16	6.54*	0.60*	340 ± 25	1.60	1.016
	(3)	1.02	1.15 ± 0.05	8.93 ± 0.11	11.40 ± 0.19	6.51 ± 0.05	0.53 ± 0.10	265 ± 31	0.76	1.081
	(4-1)	1.02	1.16 ± 0.04	7.64 ± 0.13	9.45 ± 0.18	6.61*	0.64*	307 ± 29	2.03	1.127
	(4-2)	1.03	1.05 ± 0.07	8.00 ± 0.10	11.66 ± 0.19	6.63 ± 0.04	0.43 ± 0.07	252 ± 26	1.12	1.024
	(5)	1.02	1.02 ± 0.08	9.04 ± 0.12	11.89 ± 0.19	6.50*	0.51*	336 ± 31	0.70	0.951
	(6-1)	1.01	1.12 ± 0.05	8.68 ± 0.29	6.54 ± 0.24	6.47 ± 0.08	0.79 ± 0.14	385 ± 55	2.43	0.920
	(6-2)	1.01	1.18 ± 0.08	7.39 ± 0.19	9.18 ± 0.35	6.52 ± 0.08	0.42 ± 0.18	276 ± 41	2.27	1.161
	(7)	1.03	0.86 ± 0.06	9.29 ± 0.05	13.43 ± 0.89	6.46 ± 0.04	0.44 ± 0.05	215 ± 19	0.98	1.003
*04	–	1.03	1.04 ± 0.05	8.81 ± 0.05	14.46 ± 0.14	6.53 ± 0.04	0.43 ± 0.07	180 ± 13	1.17	1.060
*06	–	1.03	0.86 ± 0.16	8.30 ± 0.08	16.53 ± 0.27	6.28 ± 0.06	0.53 ± 0.08	365 ± 29	0.35	0.991
*08	(1)	1.04	0.68 ± 0.13	9.31 ± 0.08	13.51 ± 0.14	6.28 ± 0.09	0.67 ± 0.11	291 ± 38	0.70	0.959
	(2)	1.03	0.87 ± 0.08	9.07 ± 0.08	13.81 ± 0.14	6.39 ± 0.05	0.28 ± 0.08	145 ± 17	0.69	1.071
	(3)	1.03	0.90 ± 0.08	9.11 ± 0.09	12.96 ± 0.16	6.46 ± 0.08	0.36 ± 0.12	154 ± 24	0.64	1.044
	(4-1)	1.01	1.05 ± 0.05	7.52 ± 0.24	6.81 ± 0.25	6.32 ± 0.10	0.96 ± 0.11	568 ± 78	2.72	0.971
	(4-2)	1.02	1.00 ± 0.04	7.29 ± 0.09	9.70 ± 0.13	6.61*	0.67*	381 ± 27	1.90	0.969

* The parameters were poorly constrained and were fixed.

to explain the occurrence of LMC X-4 flares. However, a detailed study is required for a more reliable interpretation.

Some authors (see, e.g., Levine et al. 2000) note a certain similarity of the observed manifestations of flaring activity in LMC X-4 (in particular, the super-Eddington character of flares) to the flares recorded in magnetars (Thompson and Duncan 1995; Kaspi and Beloborodov 2017). However, such an analysis reveals significant differences in the manifestations of flaring activity (see also Levine et al. 2000)—magnetars are characterized by ultrashort flares ($\sim$0.1–10 s in duration), a spectral hardening during flares, the absence of pulsations at the flare peak, a long period between flares, etc. This leads to the conclusion that the magnetar mechanism is unsuitable for describing the flares in LMC X-4 (Levine et al. 2000), despite the fact that the magnetic field in this system can be sufficiently strong ($>10^{13}$ G; see Shtykovsky et al. 2017).

Another possible mechanism explaining the flaring activity in LMC X-4 can be a modification of the model proposed by Shakura et al. (2012, 2013) to explain the phenomenon of SFXT flares. Indeed, comparing the parameters of flares from LMC X-4 and SFXTs, one can notice a large number of similar characteristics—close luminosities during flares, similar flare shapes and characteristic flare evolution time scales, etc. However, the SFXT mechanism suggests low quiescent luminosities, less than $L_{\rm x} \sim 10^{36}$ erg s^{-1}. At higher luminosities it is quite difficult to explain frequent flares by this model.

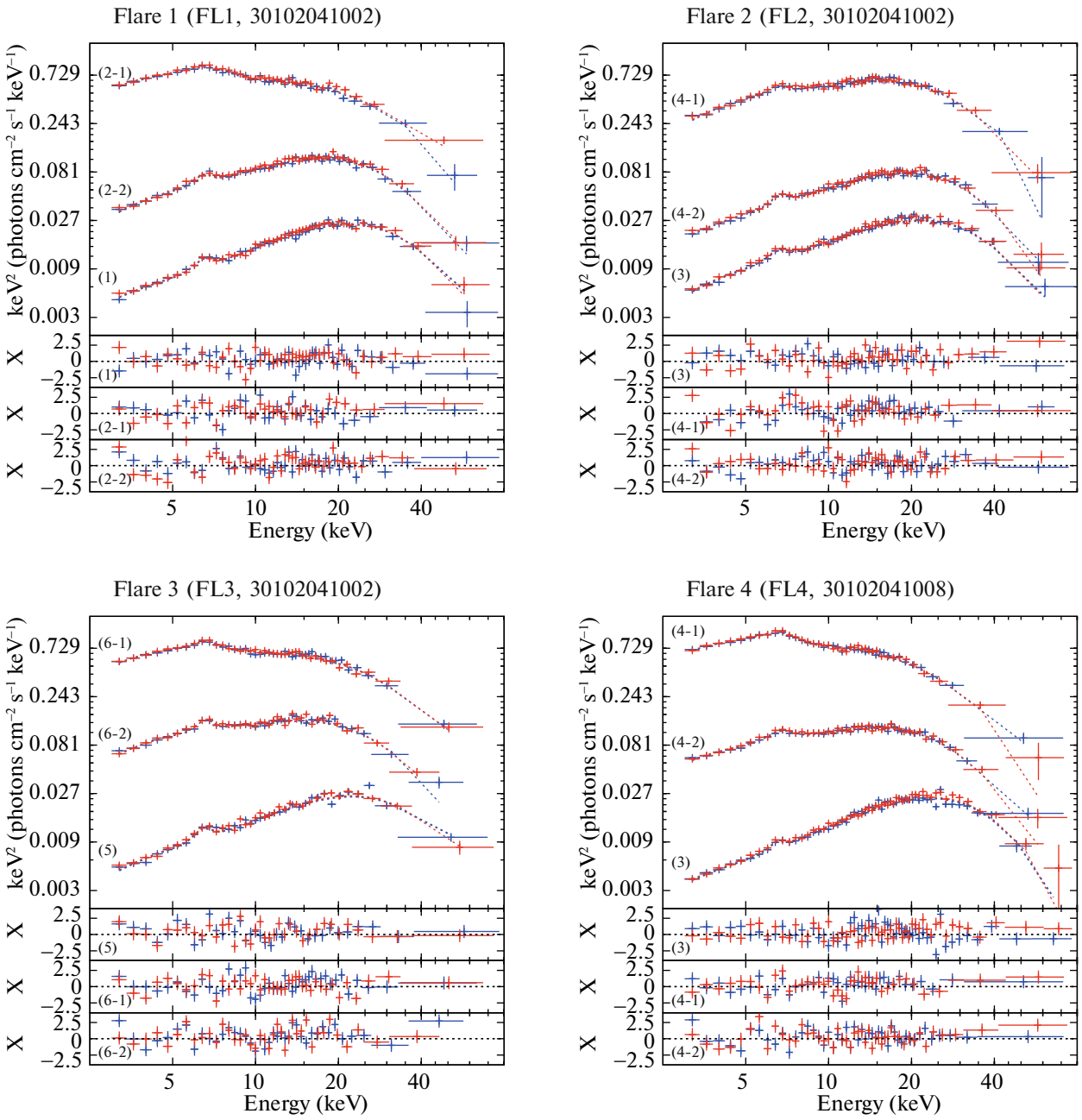

Fig. 8. (Color online) Energy spectra before, during, and after the flare; the spectra before and after the flare were constructed with coefficients of 0.1 and 0.2, respectively; the interval numbers correspond to the numbering in Figs. 1 and 2.

Changes in the Pattern of Radiation As the Luminosity Increases to Super-Eddington Values

Owing to the high sensitivity and the wide energy range of the NuSTAR observatory, it has been possible for the first time to trace the changes in the spectrum and pulse profile of the pulsar LMC X-4 in the energy range 3–79 keV when passing to the super-Eddington regime of accretion. The source spectrum both during the flares and in quiescence is well described by the thermal Comptonization model (COMPTT). The following changes in the spectrum and pulse profile were observed during the flares as the luminosity increased above $L_x \sim 6 \times 10^{38}$ erg s^{-1}:

(1) the pulse profile in the energy range 3–40 keV becomes approximately triangular (Figs. 4–6);

(2) the pulsed fraction increases with rising energy, reaching 60–70% in the energy range 25–40 keV, which exceeds considerably 6–14% in the quiescent state (Fig. 7);

(3) an increase in luminosity by more than an order of magnitude is observed at energies below

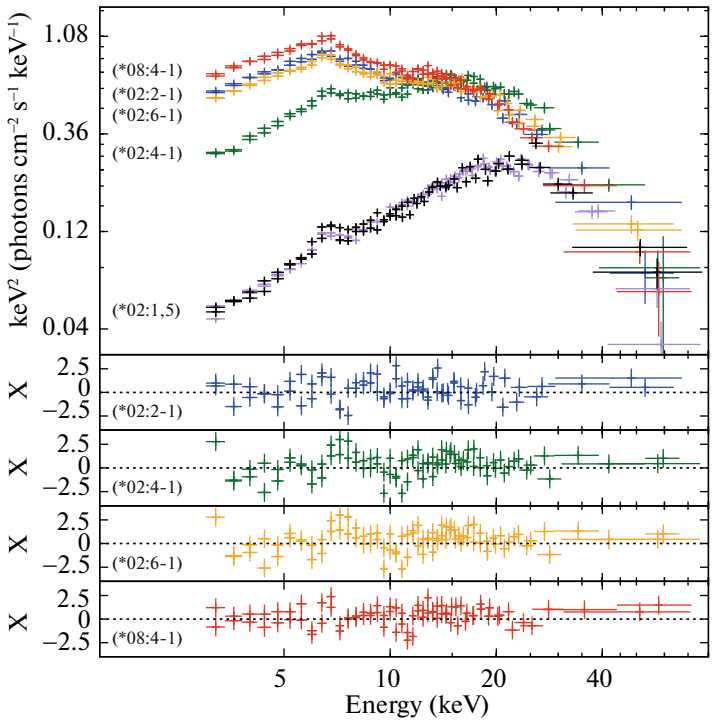

Fig. 9. (Color online) Superimposed spectra of the flares in intervals (2-1), (4-1), and (6-1) of observation 30102041002 (*02:2-1, *02:4-1, and *02:6-1) and interval (4-1) of observation 30102041008 (*08:4-1) and spectra in the quiescent state in intervals (1) and (5) of observation 30102041002 (*02:1, 5).

25–30 keV, while at higher energies both the spectrum shape and the recorded flux remain virtually unchanged (Figs. 8 and 9);

(4) an anticorrelation of the plasma temperature and the optical depth with the X-ray luminosity of the source is observed (Table 2, Fig. 10).

Many X-ray pulsars are known to exhibit a spectral hardening as the luminosity increases, and saturation and even softening of the pulsar spectrum occur when some critical luminosity is reached (Postnov et al. 2015). The characteristic luminosity at which the transition to saturation occurs is $\sim 10^{37}$ erg s^{-1}. Postnov et al. (2015) proposed an accretion column model in which such changes are explained by Compton saturation, whereby the Comptonized emission from the side wall of the accretion column is reflected from the neutron star atmosphere (see also Poutanen et al. 2013). As the accretion rate and the luminosity rise, the column height increases and the fraction of the reflected, predominantly hard component in the spectrum begins to decrease, causing the pulsar spectrum to soften. According to the standard accretion column model (Basko and Sunyaev 1975), the column height increases with rising luminosity and a fan radiation pattern is realized. For a distant observer this manifests itself in the fact that the pulse profile becomes double-peaked (Gnedin and Sunyaev 1973). Interestingly, a qualitatively similar behavior can also be explained in terms of the present-day model for the generation of X-ray pulsar radiation that takes into account the reflection of the radiation emitted by the accretion column from the neutron star surface (see Poutanen et al. (2013) and Fig. 6 in Lutovinov et al. (2015)).

For LMC X-4 we also observe a spectral softening with increasing luminosity similar to that noted in Postnov et al. (2015). However, the recorded pulse profile (triangular single-peaked) is more likely indicative of a pencil radiation pattern, suggesting a small height of the accretion column. In this case, the destruction/disappearance of the column at super-Eddington luminosities can be assumed. At the same time, the observed slight decrease in plasma temperature and optical depth is also consistent with a decrease in accretion column height, given that in the model of Postnov et al. (2015) the electrons at the outermost edges of the accretion column are the Comptonizing medium. Another possible explanation for the observed changes in the pulse profiles is the transition of the pulsar LMC X-4 to the state of an ultraluminous X-ray source (ULX), which are also characterized by single-peaked and approximately sinusoidal pulse profiles and by an increase in pulsed fraction with energy (see, e.g., Fürst et al. 2016; Mushtukov et al. 2017).

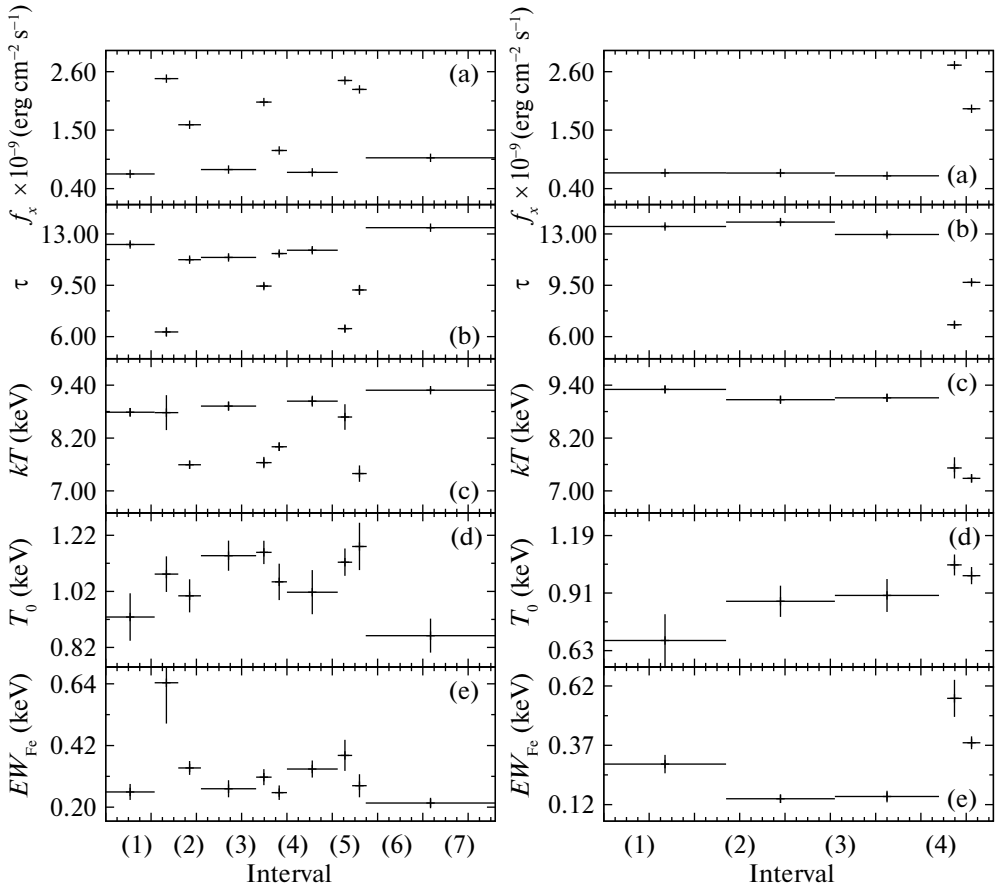

Fig. 10. Evolution of the spectral parameters in various intervals: the flux (a), the optical depth (b), the plasma temperature (c), the seed photon temperature (d), and the equivalent width of the fluorescent iron line (e) for observations 30102041002 (left panel) and 30102041008 (right panel).

ACKNOWLEDGMENTS

Shtykovsky, Lutovinov, and Molkov were supported by the Russian Science Foundation (project no. 14-12-01287). We used data from the NuSTAR observatory, a project led by Caltech, funded by NASA, and managed by NASA/JPL. The data were reduced using the NUSTARDAS package, jointly developed by ASDC (Italy) and Caltech (USA).

REFERENCES

1. M. M. Basko and R. A. Sunyaev, Astron. Astrophys. **42**, 311 (1975).
2. P. A. Boldin, S. S. Tsygankov, A. A. Lutovinov, Astron. Lett. **39**, 375 (2013).
3. E. F. Brown and L. Bildsten, Astrophys. J. **496**, 915 (1998).
4. K. Dennerl, *Proceedings of the 23rd ESLAB Symp. on Two Topics in X Ray Astronomy* (European Space Agency, 1989), Vol. 1, p. 39.
5. J. M. Dickey, F. J. Lockman, Annu. Rev. Astron. Astrophys. **28**, 215 (1990).
6. M. Falanga, E. Bozzo, A. Lutovinov, J. M. Bonnet-Bidaud, Y. Fetisova, and J. Puls, Astron. Astrophys. **577**, A310 (2015).
7. F. Fürst, D. J. Walton, F. A. Harrison, D. Stern, D. Barret, M. Brightman, A. C. Fabian, B. Grefenstette, et al., Astrophys. J. **831**, L14 (2016).
8. Yu. N. Gnedin and R. A. Sunyaev, Astron. Astrophys. **25**, 233 (1973).
9. F. A. Harrison, W. W. Craig, F. E. Christensen, C. J. Hailey, W. W. Zhang, S. E. Boggs, D. Stern, W. R. Cook, et al., Astrophys. J. **770**, 103 (2013).
10. M. H. M. Heemskerk and J. van Paradijs, Astron. Astrophys. **223**, 154 (1985).
11. V. M. Kaspi and A. Beloborodov, Astron. Astrophys. (2017, in press).
12. R. L. Kelley, J. G. Jernigan, A. Levine, L. D. Petro, and S. Rappaport, Astrophys. J. **264**, 568 (1983).
13. F. L. Lang, A. M. Levine, M. Bautz, S. Hauskins, S. Howe, F. A. Primini, W. H. G. Lewin, W. A. Baity, et al., Astrophys. J. **246**, L21 (1981).
14. A. Levine, S. Rappaport, A. Putney, R. Corbet, and F. Nagase, Astrophys. J. **381**, 101 (1991).
15. A. M. Levine, S. A. Rappaport, and G. Zojcheski, Astrophys. J. **541**, 194 (2000).

16. F. Li, S. Rappaport, and A. Epstein, Nature **271**, 37 (1978).
17. A. A. Lutovinov and S. S. Tsygankov, Astron. Lett. **35**, 433 (2009).
18. A. A. Lutovinov, S. S. Tsygankov, V. F. Suleimanov, A. A. Mushtukov, V. Doroshenko, D. I. Nagirner, and J. Poutanen, Mon. Not. R. Astron. Soc. **448**, 2175 (2015).
19. F. Melia and M. Fatuzzo, Astrophys. J. **438**, 904 (1995).
20. S. Molkov, A. Lutovinov, and M. Falanga, Astron. Lett. **41**, 562 (2015).
21. S. Molkov, A. Lutovinov, M. Falanga, S. Tsygankov, and E. Bozzo, Mon. Not. R. Astron. Soc. **464**, 2039 (2017).
22. D.-S. Moon and S. S. Eikenberry, Astrophys. J. **549**, L225 (2001).
23. A. A. Mushtukov, V. F. Suleimanov, S. S. Tsygankov, and A. Ingram, Mon. Not. R. Astron. Soc. **467**, 1202 (2017).
24. J. Neilsen, J. C. Lee, M. A. Nowak, K. Dennerl, and S. D. Vrtilek, Astrophys. J. **696**, 182 (2009).
25. K. A. Postnov, M. I. Gornostaev, D. Klochkov, E. Laplace, V. V. Lukin, and N. I. Shakura, Mon. Not. R. Astron. Soc. **452**, 1601 (2015).
26. J. Poutanen, A. Mushtukov, V. Suleimanov, S. Tsygankov, D. Nagirner, V. Doroshenko, and A. Lutovinov, Astrophys. J. **777**, 315 (2013).
27. A. E. Shtykovsky, A. A. Lutovinov, V. A. Arefiev, S. V. Molkov, S. S. Tsygankov, and M. G. Revnivtsev, Astron. Lett. **43**, 175 (2017).
28. C. Thompson and R. C. Duncan, Mon. Not. R. Astron. Soc. **275**, 255 (1995).
29. L. Titarchuk, Astrophys. J. **434**, 570 (1994).
30. S. S. Tsygankov and A. A. Lutovinov, Astron. Lett. **31**, 380 (2005).
31. R. Turolla and P. Esposito, Int. J. Mod. Phys. **22** (2013).
32. N. E. White, Nature **271**, 38 (1978).
33. J. W. Woo, G. W. Clark, A. M. Levine, R. H. D. Corbet, and F. Nagase, Astrophys. J. **467**, 811 (1996).

Translated by V. Astakhov